

# **Under-ice ambient noise in Eastern Beaufort Sea, Canadian Arctic, and its relation to environmental forcing**

G. Bazile Kinda, Yvan Simard, Cédric Gervaise, et al.

Citation: [The Journal of the Acoustical Society of America](#) **134**, 77 (2013); doi: 10.1121/1.4808330

View online: <https://doi.org/10.1121/1.4808330>

View Table of Contents: <https://asa.scitation.org/toc/jas/134/1>

Published by the [Acoustical Society of America](#)

---

## **ARTICLES YOU MAY BE INTERESTED IN**

[Arctic underwater noise transients from sea ice deformation: Characteristics, annual time series, and forcing in Beaufort Sea](#)

The Journal of the Acoustical Society of America **138**, 2034 (2015); <https://doi.org/10.1121/1.4929491>

[Underwater ambient noise on the Chukchi Sea continental slope from 2006–2009](#)

The Journal of the Acoustical Society of America **131**, 104 (2012); <https://doi.org/10.1121/1.3664096>

[Ambient Noise under Arctic-Sea Ice](#)

The Journal of the Acoustical Society of America **36**, 855 (1964); <https://doi.org/10.1121/1.1919103>

[Eastern Arctic ambient noise on a drifting vertical array](#)

The Journal of the Acoustical Society of America **142**, 1997 (2017); <https://doi.org/10.1121/1.5006053>

[Acoustic Ambient Noise in the Ocean: Spectra and Sources](#)

The Journal of the Acoustical Society of America **34**, 1936 (1962); <https://doi.org/10.1121/1.1909155>

[Measured and modeled acoustic propagation underneath the rough Arctic sea-ice](#)

The Journal of the Acoustical Society of America **142**, 1619 (2017); <https://doi.org/10.1121/1.5003786>

---

# Under-ice ambient noise in Eastern Beaufort Sea, Canadian Arctic, and its relation to environmental forcing

G. Bazile Kinda<sup>a)</sup>

*Grenoble Images Parole Signal Automatique Lab, Grenoble Institute of Technology and Centre National de la Recherche Scientifique, 11 rue des Mathématiques, 38402 Saint-Martin d'Hères, France*

Yvan Simard<sup>b)</sup>

*Marine Science Institute, University of Québec at Rimouski, 310 Allée des Ursulines, Rimouski, Quebec G5L-3A1, Canada*

Cédric Gervaise<sup>c)</sup>

*Chaire Chorus, Foundation of Grenoble Institute of Technology, 46, Avenue Felix Viallet, 38031 Grenoble Cedex 1, France*

Jérôme I. Mars

*Grenoble Images Parole Signal Automatique Lab, Grenoble Institute of Technology and Centre National de la Recherche Scientifique, 11 rue des Mathématiques, 38402 Saint-Martin d'Hères, France*

Louis Fortier

*Canada Research Chair on the Response of Arctic Marine Ecosystems to Climate Change, Québec-Océan, Department of Biology, Laval University, Québec, Quebec G1V 0A6, Canada*

(Received 8 February 2013; revised 12 May 2013; accepted 20 May 2013)

This paper analyzes an 8-month time series (November 2005 to June 2006) of underwater noise recorded at the mouth of the Amundsen Gulf in the marginal ice zone of the western Canadian Arctic when the area was >90% ice covered. The time-series of the *ambient noise* component was computed using an algorithm that filtered out transient acoustic events from 7-min hourly recordings of total ocean noise over a [0–4.1] kHz frequency band. Under-ice ambient noise did not respond to thermal changes, but showed consistent correlations with large-scale regional ice drift, wind speed, and measured currents in upper water column. The correlation of ambient noise with ice drift peaked for locations at ranges of ~300 km off the mouth of the Amundsen Gulf. These locations are within the multi-year ice plume that extends westerly along the coast in the Eastern Beaufort Sea due to the large Beaufort Gyre circulation. These results reveal that ambient noise in Eastern Beaufort Sea in winter is mainly controlled by the same meteorological and oceanographic forcing processes that drive the ice drift and the large-scale circulation in this part of the Arctic Ocean.

© 2013 Acoustical Society of America. [<http://dx.doi.org/10.1121/1.4808330>]

PACS number(s): 43.30.Nb, 43.50.Rq, 43.60.Cg [JIA]

Pages: 77–87

## I. INTRODUCTION

The Arctic Ocean is entirely covered with ice of variable thickness and age during winter (Marsan *et al.*, 2004; Maslanik *et al.*, 2011; Marsan *et al.*, 2012; Stroeve *et al.*, 2012). The seasonal extent and the ice thickness of this polar ice cap is changing rapidly in response to global warming (Polyak *et al.*, 2010; Stroeve *et al.*, 2012; Wadhams, 2012). The presence of an ice cover is responsible for particular underwater ocean-noise characteristics, relative to open-water conditions (Roth *et al.*, 2012). Diverse processes contribute to the generation of under-ice noise (Carey and Evans, 2011). The pioneer work of Milne and Ganton (1964)

(Ganton and Milne, 1965) showed that thermal ice cracking associated with air temperature fluctuations in the Arctic Ocean produces low-frequency impulses, while the interaction of the wind with the ice surface creates Gaussian noise at frequencies >1 kHz (Urick, 1984). Makris and Dyer (1986, 1991) later showed that low-frequency (1–100 Hz) under-ice noise was wind dependent, and that collisions between ice blocks and ice fracturing (Zakarauskas *et al.*, 1990) also significantly contribute to the under-ice noise. Other processes, such as ridging, shearing, and ice-mass vibrations were subsequently identified as contributors to low-frequency (<200 Hz) Arctic Ocean noise (Greening and Zakarauskas, 1992, 1994). During the Arctic Ice Dynamics Joint Experiment (AIDJEX) project, Lewis and Denner (1987, 1988a,b) highlighted correlations between sea-ice kinematic and low-frequency ocean-noise levels under the perennial ice sheet of central Beaufort Sea at different seasons. Based on cross-correlation between two sensors, they estimated spatial scales that can reach 1000 km (Lewis and Denner, 1987). They also showed correlations with wind

<sup>a)</sup>Author to whom correspondence should be addressed. Also at: ENSTA-Bretagne, 2, rue François Verny, 29200, Brest, France. Electronic mail: bazile.kind@ensta-bretagne.fr

<sup>b)</sup>Also at: Maurice Lamontagne Institute, Fisheries and Oceans Canada, 850 route de la Mer, Mont-Joli, QC G5H-3Z4, Canada.

<sup>c)</sup>Also at: GIPSA-lab, Grenoble Institute of Technology and CNRS, 11 rue des Mathématiques, 38402 Saint-Martin d'Hères, France.

speed, and with changes in air temperature and atmospheric pressure. Under-ice noise characteristics appear, therefore, to depend both on multi-scale atmospheric effects that act on the internal stress and structural integrity of the ice, and on ice drift and shearing.

The Canadian waters up to latitudes of  $\sim 74^{\circ}\text{N}$  are generally free of ice in late summer, when the extent of the Arctic sea-ice reaches its minimum in September [Fig. 1(a), for September 2005]. The marginal ice zone that lies between the perennial ice and the coast closes in during October [Fig. 1(c), for October/November 2005] (Barber *et al.*, 2012; Galley *et al.*, 2012). The maximum ice extent and thickness (Stroeve *et al.*, 2008; Stroeve *et al.*, 2012) are reached in late winter, so in March/April [Figs. 1(b), 1(d)], which is followed by the melting that is complete in July. Except for land-fast ice, the Arctic sea-ice is in perpetual motion during winter, in response to five main forcings: wind, currents, Coriolis Force, internal stress, and sea-ice surface tilt (Thorndike and Colony, 1982; Barry *et al.*, 1993; Rotschky *et al.*, 2011). In the Arctic, this motion is structured into two main circulation patterns: the Beaufort Gyre, and the transpolar drift [Fig. 1(e)]. The Beaufort Gyre is centered at about  $(80^{\circ}\text{N}, 155^{\circ}\text{W})$  (Barry *et al.*, 1993) [Fig. 1(e)]. It is anti-cyclonic (circulates clockwise), and it is the main circulation pattern of the Arctic sea-ice drift in the Canadian Basin (Stein, 1988; Aspin *et al.*, 2009; Lukovich *et al.*, 2009). This large-scale circulation pattern tends to push the ice against the Canadian Archipelago and to pile up multi-year ice in this region (Barry *et al.*, 1993). In the eastern part, northeast of Greenland, the transpolar drift forces the eventual emptying of the ice into the Atlantic, through Fram Strait (Tsukernik *et al.*, 2010; Smedsrød *et al.*, 2011) [Figs. 1(e), 1(f)]. In the western part, in the Eastern Beaufort Sea, the multi-year ice is extended westwards by the Beaufort Gyre, into a plume at the marginal ice boundary, and it is not fast to the coast in the Amundsen Gulf, where there is essentially only first-year ice [Figs. 1(c), 1(e), 1(f)] (Kwok, 2006; Barber *et al.*, 2012; Galley *et al.*, 2012).

In this paper we examine the under-ice noise from an 8-month time-series of [0–4.1 kHz] recordings using an autonomous underwater recorder in the marginal ice zone of the western Canadian Arctic. We analyze the relationships with the possible regional forcing processes, notably ice drift, wind speed, current speed, air temperature, and air pressure. To prevent the estimated noise level being dominated by nearby transient events, such as ice knocking, fracturing, cracking, shearing and ridging, we used the ambient noise level (ANL) metric, in contrast to previous studies that have worked with total ocean noise. *Ambient noise* is defined by NRC (2003), as the noise that originates from a myriad of indistinguishable sources. We used a dedicated algorithm to extract this ambient noise component from the measurements of the total ocean noise.

The next three sections present the acoustic data, the sources of the environmental variables used in the study, the numerical analysis, the results, and a discussion. A dedicated Appendix presents the details of the algorithm used to estimate the ANL and to filter out distinctive sources from the total ocean noise.

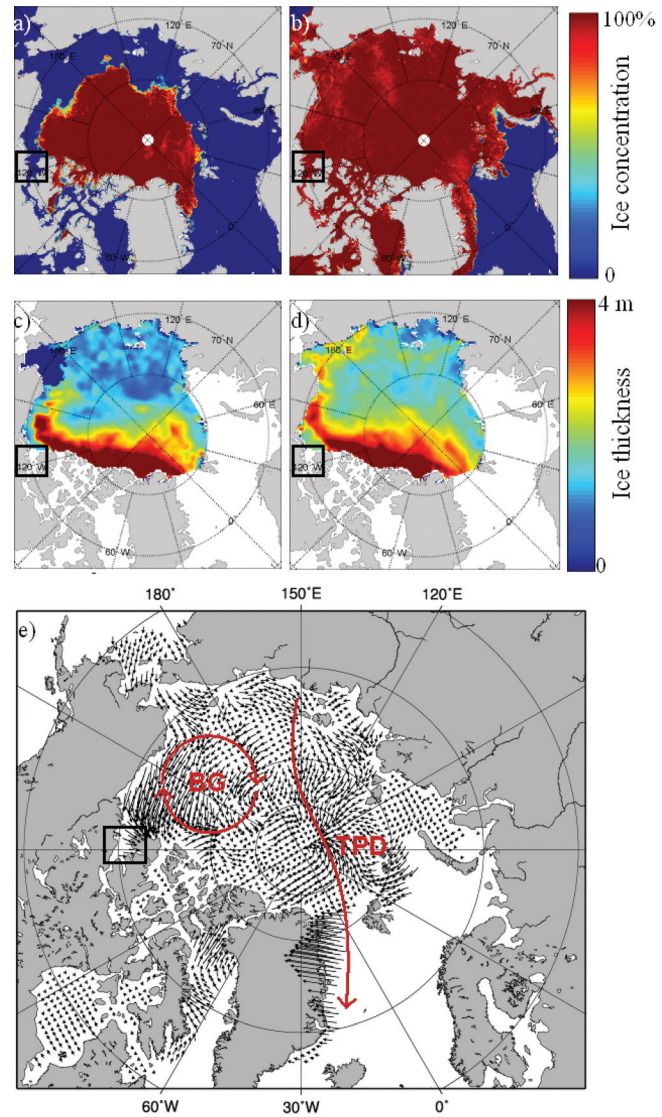


FIG. 1. Arctic ice cap characteristics (rectangle indicates the study area). (a) Sea-ice concentrations during its minimum extent in September 2005. (b) Sea-ice concentrations during its maximum extent in March 2006. (c) Ice thickness in October/November 2005, showing accumulation of multi-year ice along the Canadian archipelago. (d) Ice thickness during the winter (February/March 2006), showing its extension west, up to the Alaskan coast. (e) Arctic Ocean dominant current structure, showing the Beaufort Gyre (BG) and the transpolar drift (TPD), and an example of the ice-drift vector fields on December 26, 2005. Data are from the NSIDC.

## II. MATERIALS AND METHODS

### A. The dataset

Within the framework of the NSERC NCE ArcticNet<sup>1</sup> research program, an oceanographic mooring with a suite of instruments was deployed in 397-m-deep water at the mouth of the Amundsen Gulf ( $71^{\circ}00.493'\text{N}$ ,  $126^{\circ}04.230'\text{W}$ ) in the Eastern Beaufort Sea (Fig. 2), from September 9, 2005, to October 2, 2006. An AURAL-M2, autonomous underwater recorder (Multi-Electronique, Rimouski, QC, Canada),<sup>2</sup> was attached to the mooring line at a depth of  $\sim 50\text{ m}$ , thus positioned in the upper part of the water column where the acoustic signals converge due to the general upward refracting sound profile in the Arctic (Urick, 1983). A 300-kHz ADCP (Acoustic Doppler Current Profiler, Teledyne RDI,

Poway, CA, USA) was attached at  $\sim$ 93-m in depth to provide the current-speed profile in the upper water column, with 8-m bin resolution every 20 min. The AURAL was programmed to record acoustic data for 7 min  $h^{-1}$  with 16-bit resolution and 8192-Hz sampling rate of the low-pass anti-aliasing filtered signal, which provided a usable acoustic bandwidth of [ $\sim$ 4–4096 Hz]. The receiving sensitivity of the hydrophone (HTI 96 MIN; High Tech, Inc., Gulfport, MS, USA)<sup>3</sup> used with the AURAL was obtained from experimental calibrations conducted at the Defense Research and Development of Canada–Atlantic calibration facility (Dartmouth, NS, Canada). The receiving sensitivity is flat at  $-164 \pm 1$  dB re 1 V  $\mu\text{Pa}^{-1}$  over the bandwidth used in the present work. The hydrophone and the amplification setting used (17 dB) produced a self-noise of  $\sim$ 0.06% of the dynamic range, which corresponds to a white-noise floor of  $\sim$ 52 dB ref 1  $\mu\text{Pa}^2 \text{ Hz}^{-1}$  from 0 to 4096 Hz. The AURAL also recorded its depth and the water temperature at the beginning of every duty cycle.

Hourly and daily meteorological variables (wind speed, air pressure, air temperature, snow and rain fall) were obtained from the Environment Canada<sup>4</sup> Cape Parry weather station in the Amundsen Gulf ( $70^{\circ}00.17'\text{N}$ ,  $124^{\circ}00.72'\text{W}$ ), which is  $\sim$ 80 km from the recording station (Fig. 2). Unfortunately, during a period of  $\sim$ 23 days, the Cape Parry station was not operating, and so the meteorological data were taken from the Sachs Harbor weather station, on the northern side of the Amundsen Gulf (Fig. 2,  $\sim$ 100 km from the recording station). These data showed high correlation with the Cape Parry series.

The daily sea-ice concentration time-series were derived from the Advanced Microwave Scanning Radiometer of the Earth Observing System (AMSR-E) 89-GHz-channel satellite (Kaleschke *et al.*, 2001; Spreen *et al.*, 2008), as obtained with a  $6.25 \text{ km} \times 6.25 \text{ km}$  resolution from the Integrated Climate Data Centre (University of Hamburg, Germany).<sup>5</sup> Ice thickness maps were derived from the Ice, Cloud, and Land Elevation Satellite (ICESat) data (Rotschky *et al.*, 2011), and were obtained from the same source with a  $25 \text{ km} \times 25 \text{ km}$  resolution for October–November 2005 and for February–March 2006. Daily ice-drift vector time-series were calculated using gridded satellite-derived ice motion

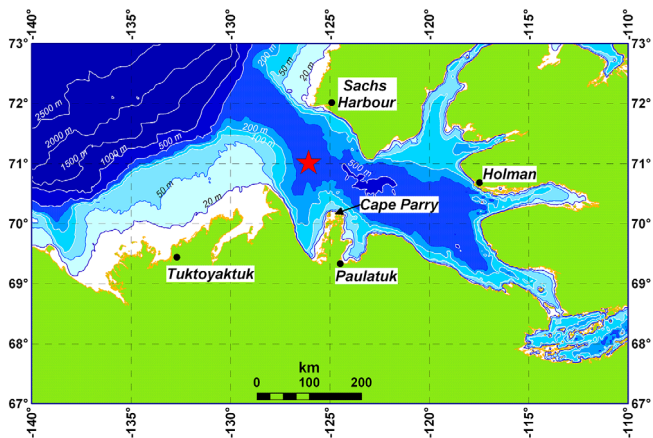


FIG. 2. (Color online) Map of the study area, showing the bathymetry and the locations of the recording station in the Amundsen Gulf and the coastal weather stations of Cape Parry and Sachs Harbor.

and the Arctic Buoy Program data (Fowler, 2003; Maslanik *et al.*, 2011), and were obtained with a  $25 \text{ km} \times 25 \text{ km}$  resolution from the National Snow and Ice Data Center (NSIDC; University of Colorado, Boulder, CO, USA).<sup>6</sup>

## B. Data analysis

The raw acoustic recordings were first converted to instantaneous sound pressure levels using the AURAL analog-to-digital conversion parameters, the gain, and the hydrophone receiving sensitivity calibration curve. Hourly ambient-noise spectra with an 8-Hz resolution were then estimated using a robust ambient-noise estimator. The algorithm assumed that the ambient noise in each frequency band was Gaussian and stationary and thus can be estimated from the low levels of the cumulative density function (CDF) of the measured ocean-noise levels, as computed with a high-resolution (62.5-ms time window) spectrogram (1024-point Hanning window, with 50% overlap). Working with the low percentiles of ocean noise for estimating ambient noise allows the filtering out of loud transients, which correspond to distinguishable nearby acoustic events (see Appendix for more details). As in other studies (e.g., Lewis and Denner, 1987), low frequencies were sometimes contaminated by a periodic strum from the mooring. In our year-round dataset, such contamination occurred during 6.70% of the annual time-series, 13.10% during the open-water period, and 2.20% during the ice-covered period. For fixed mooring on a vertical line, strum noise is often pulsed and contaminates acoustic recordings from low to high frequencies. A supervised signal processing tool (not shown) was developed based on these properties, to identify the contaminated time-frequency bins, which were often patterned with tractable beats of a few seconds. The contaminated time-frequency bins were tagged as missing values. Their missing spectral levels were estimated for each time step using a least-square exponential fit adjusted to the uncontaminated part of the estimated power spectrum density (PSD). Tests with uncontaminated signals showed the high correlation of the fit with the actual spectral levels, with no bias. The low levels of under-ice ambient noise at frequencies  $>500$  Hz sometimes reached the detection floor ( $\sim$ 53 dB re 1  $\mu\text{Pa}^2 \text{ Hz}^{-1}$ ) of our 16-bit dynamic range instrument. The analyses of the relations between the ANL and the environmental variables were therefore limited to the [10–500 Hz] low-frequency band. They included correlations and principal component analysis (PCA) [Legendre and Legendre (1998)] using both hourly and daily data. The PCA was performed on correlation matrices so that all of the variables considered had the same weight in the analysis. The daily correlation with the current speed used the low-pass filtered current, with  $<25$ -h components removed, to eliminate the tidal fluctuations, for which the maximum daily period is  $\sim$ 24 h 50 min. The daily mean ice drift at the station was the average of the drift vector grid within a 100-km radius of the station, which covered about the full width of the mouth of the Amundsen Gulf at this location. To locate the regional sourcing area of the ambient noise, the correlations were computed for all of the nodes of the ice-drift vectors grid over the entire Arctic Ocean.

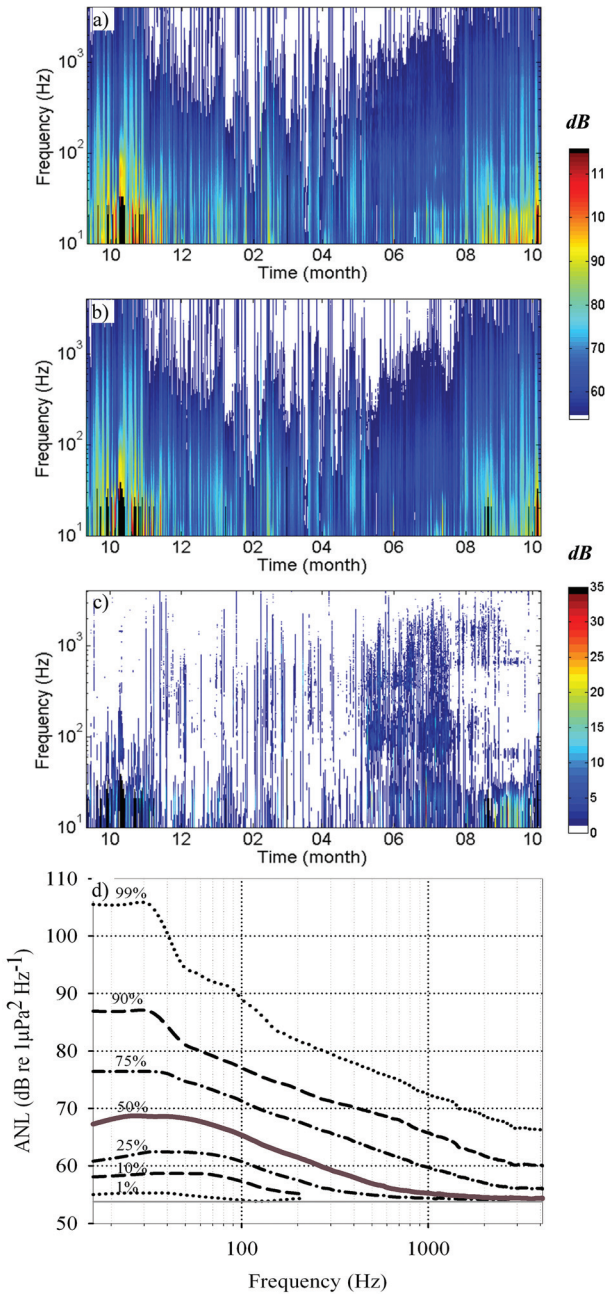


FIG. 3. Annual spectrograms of hourly spectral levels of (a) total ocean noise; (b) ANL; and (c) their ratio. (d) Percentiles of hourly spectral levels of the under-ice ANL, from November 6, 2005, to June 23, 2006. Black pixels in (a), (b), and (c) correspond to time-frequency bins affected by strum; white pixels correspond to bins with levels below the instrument floor in (a) and (b), and to a ratio of 1 (0 dB) in (c).

These correlations were computed for different percentiles of the daily CDF of the hourly estimated [10–500 Hz] ANL.

### III. RESULTS

The spectrogram that shows the annual variations of the total ocean-noise spectral levels [Fig. 3(a)] indicates the predominance of low-frequency noise with a bandwidth of a few hundred Hz and generally low noise levels above 1 kHz, except during the open-water period (from September 9 to October 28, 2005, and from July 26 to October 2, 2006), the ice formation period (October 29 to November 5, 2005), and

the ice-cover break-up (June 24 to July 25, 2006). Ambient noise contributed to a large part of the ocean noise [Fig. 3(b)] as shown in the general spectrogram pattern, although the ratio of ocean-noise/ANL [in dB; Fig. 3(c)] shows evidence of common events of transient noise that exceeded 0 dB and lasted for a few hours, especially at the beginning and the end of the ice-covered period. Most of the time, the high-frequency part of the under-ice ANL reached the measurement floor [Figs. 3(a), 3(b)] and truncated the CDF of the PSDs below the 50th percentile above 500 Hz, and the 75th percentile above 3 kHz [Fig. 3(d)]. The daily median ANL over the annual cycle was strongly negatively correlated with the presence of an ice cover, as given by the ice concentrations in a radius of 100 km around the station (Pearson  $r = -0.66$ ,  $p < 0.001$ ). This strong under-ice/open-water difference is presented in a companion paper.

Based on a 90% ice coverage criterion, the 230-days under-ice period at the station started on November 6, 2005, and ended on the June 23, 2006 [Fig. 4(a)]. The local ice concentration was often <100% and showed notable 1–3-day durations of clear water and leads, which reduced the ice concentration down to 89% (e.g., February 13, 2006). The air temperature oscillated around a mean of  $-20.5^{\circ}\text{C}$ , from  $-36.4$  to  $-6.5^{\circ}\text{C}$ , until the end of April, which was then followed by a steady rise that reached  $>0^{\circ}\text{C}$  temperatures after May 11, 2006; this corresponded to the start of the ice-cover break-up [Fig. 4(b)]. The daily pressure levels showed regular changes, with higher amplitudes before the steady rise in temperature in spring [Fig. 4(c)]. The PSD of this pressure time-series showed peaks at periods of 7 days and 15 days,

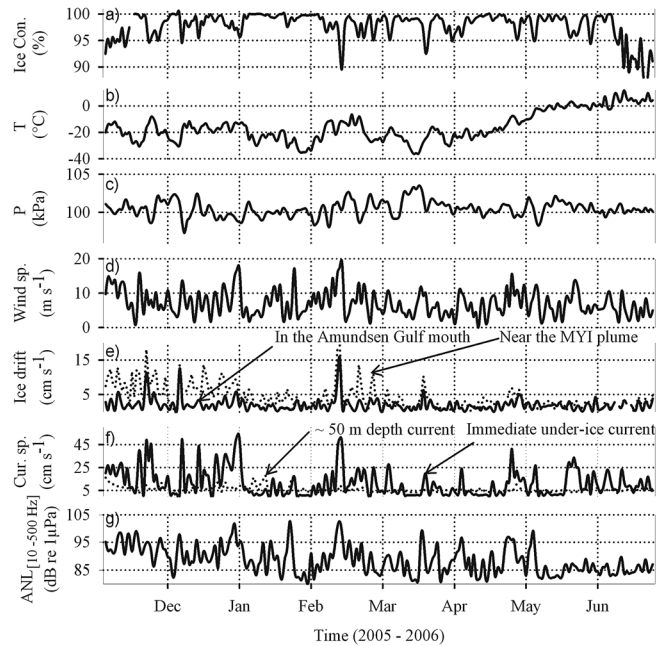


FIG. 4. Time-series (daily medians) of the environmental variables and the under-ice [10–500 Hz] ANL at the mouth of the Amundsen Gulf in winter 2005–2006. (a) Local ice concentration (100-km radius around the recording station). (b) Air temperature. (c) Air pressure. (d) Wind speed. (e) Ice-drift speed in the Amundsen Gulf (solid line) and in the multi-year ice plume off the Gulf (dashed line). (f) *In situ* current speed, showing the immediate under-ice current (solid line) and the ~50 m depth current (dashed line). (g) Broadband sound pressure level of the [10–500 Hz] ANL.

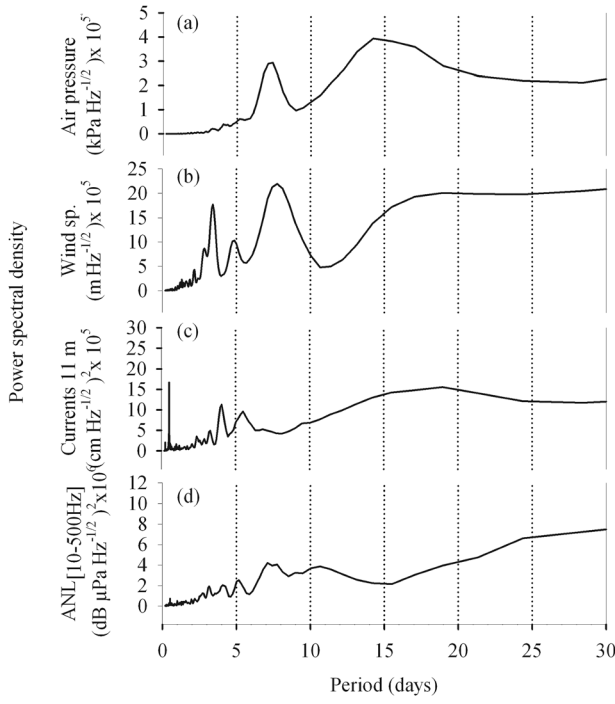


FIG. 5. PSDs of the hourly time-series presented in Fig. 4. (a) Air pressure. (b) Wind speed. (c) Currents at 11 m. (d) Broadband sound pressure level of the [10–500 Hz] ANL.

which corresponded to the local passing of depressions [Fig. 5(a), Table I]. The median daily wind speed also showed regular fluctuations, with the maximum speed reaching  $18.6 \text{ m s}^{-1}$  (37 kt) [Fig. 4(d)]. The PSD of the time-series indicated that the recurrences were mainly at periods of 4 days and 7 days, with possible larger-scale events [Fig. 5(b), Table I]. The strong winds were mainly directed along the mean coastline [ $90^\circ$  or  $270^\circ$ ; Fig. 6(a)].

The ice drift in the mouth of the Amundsen Gulf averaged  $2.1 \pm 1.8 \text{ cm s}^{-1}$ , with peaks that reached  $15.3 \text{ cm s}^{-1}$  [Fig. 4(e), solid line]. Off the Amundsen Gulf, in the multi-year ice plume area, the mean drift was higher and the fluctuations were more frequent and larger, until the beginning of the steady temperature rise in April. In contrast to the previous atmospheric environmental variables, these fluctuations did not show strong periodicity, as seen from autocorrelation and/or spectral analyses (not shown). As for the wind, the PDF of the ice-drift direction had two modes, one at

TABLE I. Periods corresponding to significant peaks in the spectra of the hourly time-series of under-ice [10–500 Hz] ANL and environmental variables, with their interpretation.

Variable	Time period (days)				
	0.26	0.52	~4	~7	~15
[10–500 Hz] ANL				x	
Air pressure				x	x
Wind			x	x	
Raw currents at 11 m	x	x	x		x
Interpretation	Tidal $M_4$	Tidal $M_2$	Storm	Storm	Tidal $M_{SF}$

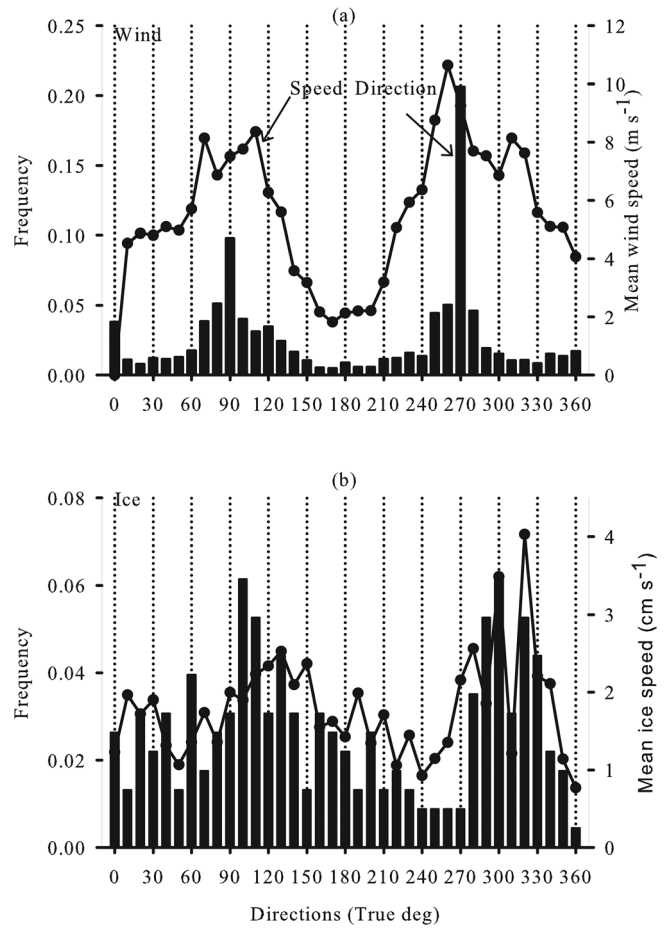


FIG. 6. Proportion of time (bars) and corresponding mean speed (lines) as functions of the direction the mean hourly wind is blowing to (a) and the ice drift within 100-km radius of the recording station (b), for the period of November 6, 2005, to June 23, 2006, as shown in Fig. 4.

$\sim 100^\circ$ – $110^\circ$ , and a second in the opposite direction, at  $\sim 280^\circ$ – $300^\circ$ , which corresponded to the strongest ice-drift speed [Fig. 6(b)]. These two modes correspond to the in and out directions of the Amundsen Gulf. The modes in ice drift direction are offset by  $\sim 10^\circ$  when the wind is directed toward the Amundsen Gulf and by  $\sim 30^\circ$  when the wind is blowing in the opposite direction. The immediate under-ice raw currents (in 7–15 m bins) averaged  $11.0 \pm 11.7 \text{ cm s}^{-1}$  and showed occasional stronger pulses that exceeded  $30 \text{ cm s}^{-1}$  [Fig. 4(f), solid line]. As expected, the raw current fluctuations were strongly related to the tidal forcing, at typical periods of  $\sim 6$  h ( $M_4$ ), 12 h ( $M_2$ ), and 14 days ( $M_{SF}$ ) [Fig. 5(c), Table I]. The currents at the depth of the AURAL recorder ( $\sim 50$  m) were 1.9-fold lower, with a mean of  $5.82 \pm 2.63 \text{ cm s}^{-1}$  [Fig. 4(f), dashed line], and were also tidally modulated.

The under-ice [10–500 Hz] ANL daily median oscillated by  $\sim 8$  dB, between  $84.6 \text{ dB}$  to  $102.5 \text{ dB}$  re  $1 \mu\text{Pa}$ , before the ice-melt in May–June, when the amplitude of the fluctuations decreased to  $\sim 2$  dB [Fig. 4(g)]. The PSD peaks of the under-ice ANL indicate recurrences at 7-day periods [Fig. 5(d), Table I]. High ANLs sometimes co-occurred with noticeable events in ice cover, drift, wind, and immediate under-ice currents [e.g., Figs. 4(a), 4(d), February 13, 2006].

As the ANL is assumed to depend on environmental forcing, PCA analysis was performed to see how the

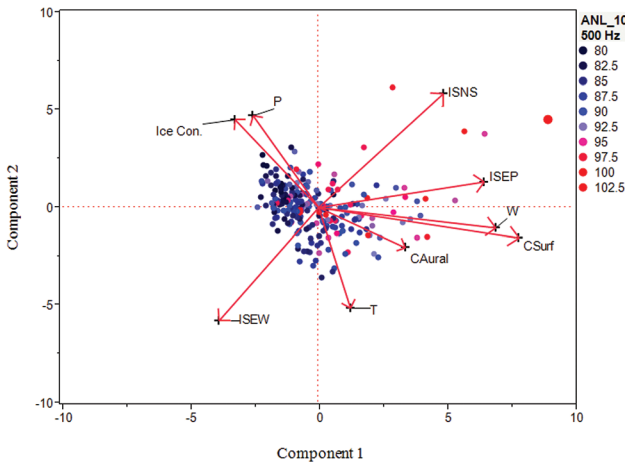


FIG. 7. Scatter plot of the PCA factor scores in the spaces of the first two principal components, along with the factor loadings for each environmental variable. Color scale indicates the daily median under-ice [10–500 Hz] ANL. Larger dots represent several points. Ice Con., ice concentration; P, air pressure; ISNS, ice speed north-south component, with northwards positive; ISEW, ice speed east-west component, with eastwards positive; ISEP, ice speed; W, wind speed; CSurf, current speed at 11 m; CAural, current speed at 51 m; T, air temperature.

environmental conditions, which were represented by the combination of the atmospheric, ice and underwater variables, were structured within the dataset, and if the ANL was responding to this structure. This is revealed by color mapping the ANL in the space of the principal components of the environmental variables (Fig. 7). The first two principal components explained 51% (first component, 30.4%; second component, 20.30%) of the total environmental variance. The overlaid plot of factor loadings in the two-component plan indicates that the noise-separating first principal component increased when the wind, ice, and current speeds increased. The second component opposes the air temperature and ice drift in the eastern direction and aligns with air

pressure, ice concentration, and ice drift in the northern direction. The first principal component separates the low-ANL observations, which were mainly in the left half space, from the high-ANL observations. High ANLs were observed during low ice concentration, low air pressure, high wind, currents, and ice drift, in particular when this drift was directed towards the northwest; i.e., out of the Amundsen Gulf. Conversely, low ANLs were more frequently observed during high ice concentration, high air pressure, low wind, low currents, and when the ice was drifting towards the Amundsen Gulf.

Pearson correlations between the [10–500 Hz] ANL and the environmental variable pairs (Table II) indicate that the ANL was strongly positively correlated with this [wind/ice drift/surface currents] triad (Pearson  $r$ : 0.37, 0.57, 0.45, respectively). The ANL tended to increase with northwards and westwards drift. The ice-drift magnitude was positively correlated with wind speed and with immediate under-ice currents, with these latter two variables strongly correlated (Pearson  $r$  = 0.72). The ice concentration during winter was negatively correlated with air temperature, which contributed little to explain the ANL variance, and with immediate under-ice currents. Correlating the ANL with hourly changes in air temperature or pressure (not shown) did not improve the correlation coefficients. The correlation of the ANL with daily changes in ice drift was also investigated (not shown), which was not significant.

Correlations of the under-ice [10–500 Hz] ANL with ice-drift time-series at every node of the entire grid over the Arctic Ocean basin located the maximum in a ~500-km-wide to 1000-km-wide area of the Eastern Beaufort Sea (Fig. 8). The core of maximum correlation was located northwest of the Amundsen Gulf, at ~300 km from the recording station in the direction of the gulf axis. The magnitude of the correlation at the core decreased slightly with the higher percentiles of the daily CDF of the hourly estimated [10–500 Hz] ANL.

TABLE II. Pearson correlations between under-ice [10–500 Hz] ANL and daily median and environmental variables. Underlined:  $p < 0.05$ ; bold:  $r^2 \geq 0.10$ .

Variable	Currents				Ice			Air		
	51 m	11 m	drift east	drift north	drift 100 km	drift 300 km	conc.	wind speed	press.	
<b>ANL</b>										
B1	<u>0.28</u>	<b>0.45</b>	-0.18	0.29	<b>0.38</b>	<b>0.57</b>	-0.09	<b>0.37</b>	-0.07	-0.15
Air	temperature	-0.07	<u>0.21</u>	0.04	-0.14	0.04	-0.08	<b>-0.44</b>	0.04	<u>-0.17</u>
	pressure	<u>-0.24</u>	<u>-0.26</u>	<u>-0.20</u>	0.10	-0.03	<u>-0.14</u>	0.07	<u>-0.23</u>	
	wind	<u>0.20</u>	<b>0.72</b>	<u>-0.17</u>	0.22	<u>0.27</u>	<b>0.40</b>	<u>-0.20</u>		
Ice	concentration	-0.11	<b>-0.34</b>	0.00	0.03	<u>-0.18</u>	<u>-0.14</u>			
	drift 100 km	<u>0.26</u>	<b>0.53</b>	<u>-0.23</u>	<b>0.38</b>	<u>0.63</u>				
	drift 300 km	0.09	<b>0.41</b>	<u>-0.43</u>	<b>0.59</b>					
	drift north	0.04	<u>0.30</u>	<b>-0.63</b>						
	drift east	0.08	<u>-0.23</u>							
<b>Currents</b>										
	11 m	<u>0.25</u>								

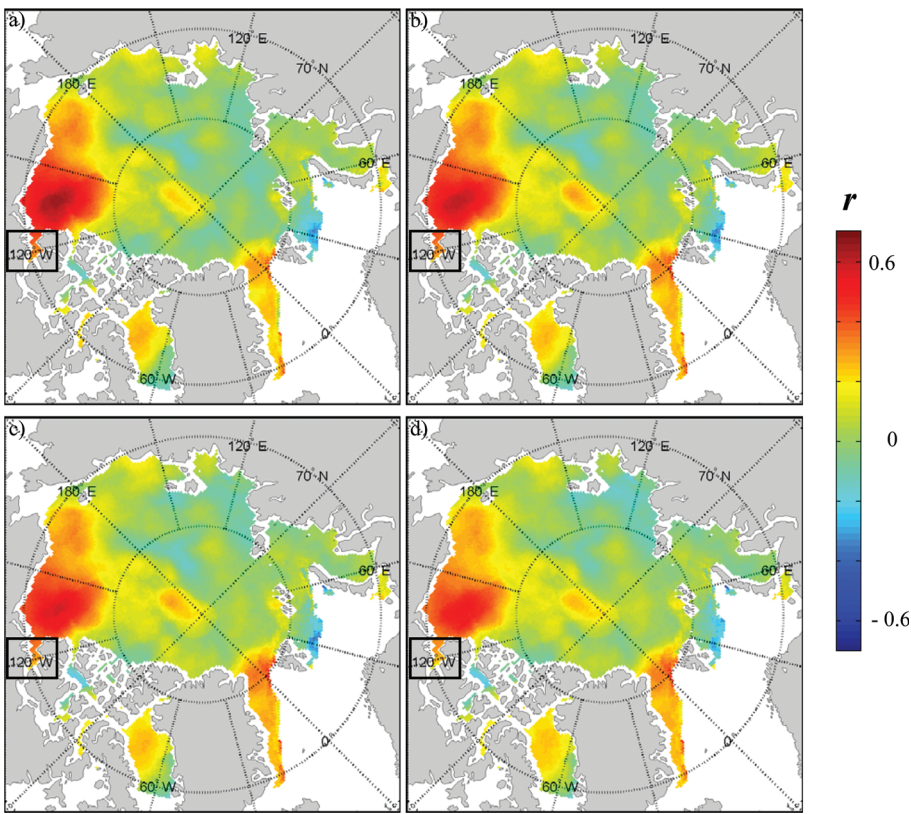


FIG. 8. Maps of the correlations (Pearson  $r$ ) between the daily under-ice [10–500 Hz] ANL and Arctic ice-drift magnitudes. The correlations are shown for different percentiles of the daily CDFs of the hourly [10–500 Hz] ANL. (a) 10th percentile. (b) 25th percentile. (c) 50th percentile. (d) 75th percentile.

There was good spatial continuity within the ice-drift field over a radius of  $\sim 250$  km from the location of the correlation core, as the correlation map indicates (Fig. 9).

#### IV. DISCUSSION

The present acoustic dataset was collected from a near-surface (50 m) portion of the water column, where acoustic

signals converge due to the upward refracting sound-speed profile. The measurements were taken near the mouth of the 550-km-long Amundsen Gulf. To our knowledge, this is the first long-term time-series that covers an entire annual cycle in this part of the Arctic Ocean. Another long acoustic time-series was collected near the ocean floor, at a depth of 235 m, at the Chukchi Sea shelf slope,  $\sim 1200$  km west of our station, in the years following our measurements (Roth *et al.*, 2012).

Ocean-noise levels are the sum of the slowly changing ambient background and the stronger transient sources, which dominate the root-mean-square sound pressure level in areas where their occurrence is high. Such strong acoustic events are common under ice, due to ice fracturing and movement (e.g., Pritchard, 1990; Xie and Farmer, 1991, 1992). Under-ice ocean noise levels are therefore strongly imprinted by local events, and are then representative of limited local areas of the three-dimensional volume of the regional ocean basin. For noise-level assessments and comparisons at larger scales, the contribution of strong transient sources should preferably be removed. In the present study, we propose a systematic method to objectively estimate the ambient-noise component from the total ocean noise, as defined by NRC (2003).

At low frequencies ( $<\sim 100$  Hz), contamination of the recorded acoustic signal by vibrations of the hydrophone and strum from the deployment line is frequent (cf. Lewis and Denner, 1987), and these are often pulsed for fixed deployments, because of the natural variability in instantaneous current forcing. This makes the collection of clean low-frequency acoustic data difficult from fixed moorings. We encountered this difficulty especially during the open-water

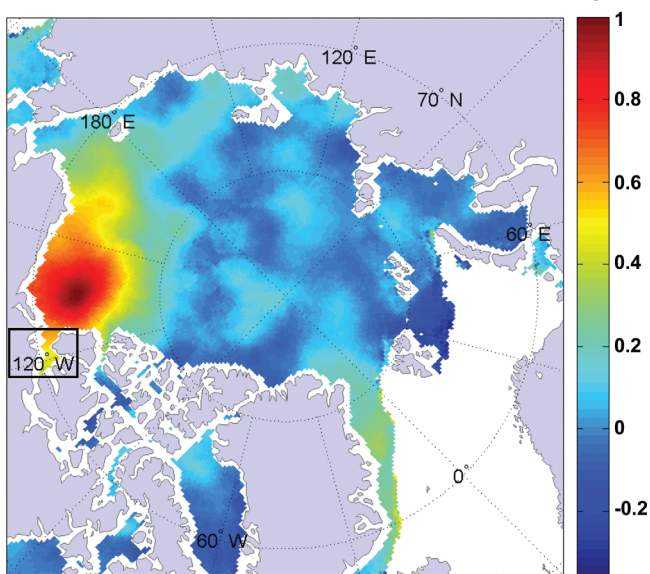


FIG. 9. Map of correlations (Pearson  $r$ ) between the ice drift time-series at the location of maximum correlation in Fig. 8 and the ice-drift time-series at other nodes of the ice-drift grid, showing the large-scale continuity in the regional ice drift.

season, and much less frequently during the ice-covered period. We made a special effort to detect and filter out these low-frequency-contaminated data, and to estimate the noise levels in the missing time-frequency bins by PSD extrapolation. The low correlation of the ANL with the current speed at the depth of the instrument, compared to the high correlation with the immediate under-ice current speed, supports the efficiency of our handling of this interference from pseudo-noise induction due to flow and strum. We are therefore confident that the data presented here are not significantly affected by strumming interference.

The measured under-ice noise levels sometimes reached the instrument floor during the ice-covered period, even below 500 Hz. This affected the lowest percentiles of the [10–500 Hz] ANL CDF, but not the median level used in the analysis [Fig. 3(d)]. The lowest measured [10–500 Hz] ANLs were therefore clipped, but not severely, because of the dominant contribution of the unaffected lowest frequency (<100 Hz) noise to the [10–500 Hz] ANLs [Fig. 3(d)].

As the ice cover formed in November, the underwater noise level in the Amundsen Gulf decreased to a minimum under consolidated ice during the winter period. Such effects of the ice cover on underwater noise levels have been observed in other seasonally ice-covered Arctic and Subarctic basins (Roth *et al.*, 2012). Seasonal modulation of the ocean noise has also been observed under perennial ice during summer, fall and winter in response to the seasonal heat cycles that affect ice motion and fracturing (Lewis and Denner, 1987). This strong seasonal modulation was observed in both the ocean and ambient noise components. This is due to the strong dominance of the ANL contribution relative to the hourly averaged contribution of transient events, which exceeded 1.4 dB only 10% of the time over the [0.01–4.1 kHz] band for the entire 13-month time-series [Figs. 3(a)–3(c)]. The use of ocean noise instead of ambient noise reduces the strength of the correlations and the clarity of the results presented here, although the general conclusions remain the same.

The estimated under-ice ANL was centered around 65 dB re  $1 \mu\text{Pa}^2 \text{Hz}^{-1}$  at 100 Hz, and half of the values were included within a 10-dB envelope around this median. This differs by only 1–3 dB from the under-ice ocean noise observations from March and May 2009 in the Chuckchi Sea slope region, despite the different depth of the recordings (235 m) and the different period [see Figs. 3(b), 3(c) in Roth *et al.*, 2012]. The spectral slopes between 100 and 1000 Hz for the same two sets of observations are also very similar at  $\sim -10$  dB per decade. The total envelope of our ANL observations at 100 Hz is 36 dB (first to 99th percentiles), while Roth *et al.* (2012) reported 34 dB (March 2009). At lower frequencies, however, our first percentile of 55 dB re  $1 \mu\text{Pa}^2 \text{Hz}^{-1}$  at 10 Hz is 17 dB lower than that reported by Roth *et al.* (2012). The 10-Hz medians also differ by the same amount (67 vs 82–88 dB re  $1 \mu\text{Pa}^2 \text{Hz}^{-1}$ , respectively). Our measurements in this low-frequency (<100 Hz) band, however, agree with the range of under-ice values published for the Arctic by Ganton and Milne (1965) and by Lewis and Denner (1987) for 32 Hz, but they do not agree for 10 Hz.

The correlations and PCA analyses show that the [10–500 Hz] ANL in the mouth of the Amundsen Gulf does

not significantly respond to the air temperature and pressure, nor to their temporal gradients. This indicates that the main forcing for the ANL was not local short-term thermal ice cracking and fracturing that was due to meteorologically forced internal ice stress, contrary to the expectations for total ocean-noise levels based on the studies of Greene and Buck (1964), Makris and Dyer (1986), and Ganton and Milne (1965). This is likely due to the fact that our ANL estimates exclude transient events, in contrast to the total ocean noise of the other studies, and consider a longer time period (230 days) compared to the short time-series of the other studies (from 1 to 24 days). In addition, since these studies from the early 1960s, global warming has forced drastic changes in the Arctic ice sheet, which has resulted in a decrease in the multi-year ice thickness and an increase in the ice-drift speed (Rampal *et al.*, 2009; Weiss *et al.*, 2009; Rampal, 2011). These changes are likely to impact upon the ambient-noise production mechanisms, and consequently on the ambient-noise multidimensional structure. The strongest correlations of the ANL with environmental variables were due to the inter-correlated triad [wind/ice drift/surface currents]. As sea-ice motion is a response to geostrophic winds, the ice pack generally moves at  $\sim 0.77$  to  $\sim 2\%$  of the surface wind speed (Thorndike and Colony, 1982; Kimura, 2004). As surface currents are driven by the ice motion (Thorndike and Colony, 1982; Nakayama *et al.*, 2012), this correlation triad is consistent with our knowledge of the functioning of this physical process. The correlation with the ANL therefore indicates the dominant contribution of ice drift to the regional ANL.

The correlation maps show that the relation between the ANL and the ice drift was not local, but was distant from our recording station by  $\sim 300$  km. The correlation core was located within the plume of multi-year ice that was moving westerly off the mouth of the Amundsen Gulf [Figs. 1(c) and 1(d)]. The correlations of the ANL with the local ice drift were positive with northwestwards drift, and therefore along the direction of the multiyear ice-plume displacement, which defines the regional momentum. Strong noise appears to be associated with westerly pulsed advances of this plume along the Beaufort Gyre, which entrains the local ice covering the mouth of the Amundsen Gulf westwards and northwards. The movement of this plume, which averaged  $4.1 \pm 3.5 \text{ cm s}^{-1}$  and peaked at  $19.3 \text{ cm s}^{-1}$  [Fig. 4(e), dashed line], is responding to the frequent  $180^\circ$  shifts in the dominant winds aligned along the coastline. The ice field at the mouth of the Amundsen Gulf appears to also respond to this wind forcing, moving in and out of the Gulf, likely guided by the topographic direction of the mouth of the Gulf. The fact that the offset of the ice drift direction relative to the wind direction is lower when the drift is toward the coasts indicates a guiding from the coastline.

The possibility that the source of the measured ANL is located in the above area of the maximum correlation core within the multi-year ice plume is plausible. The median under-ice ANL at the recording station was 65.6 dB re  $1 \mu\text{Pa}^2 \text{Hz}^{-1}$  at 100 Hz. The transmission loss (TL) from a distant source in the marginal ice zone of the Beaufort Sea can be approximated by  $20 \log_{10}(D) + 10 \log_{10}(R-D)/D$ ,

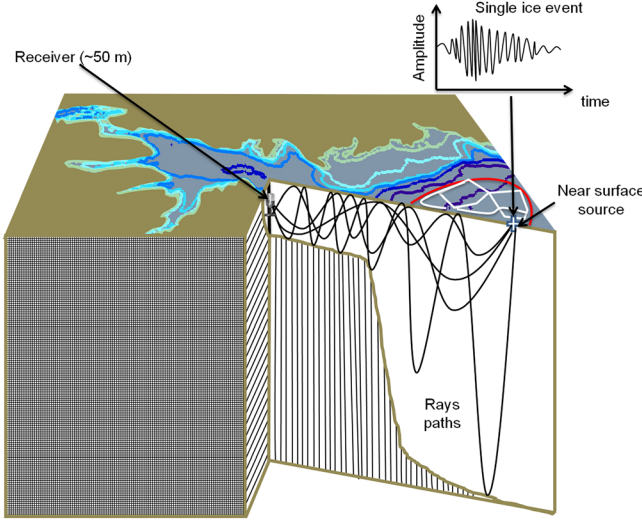


FIG. 10. (Color online) Schematic representation of the ocean-noise propagation from the multi-year ice plume that is drifting westerly from offshore Beaufort Sea to the 50-m deep recording location on the shelf in the Amundsen Gulf.

where  $D$  is the water depth and  $R$  is the source-to-receiver range, as indicated by the study of [Milne and Ganton \(1964\)](#) within a similarly exposed fjord (McClure Strait, Melville Sound) located to the north of the Amundsen Gulf. With  $D = 2.5$  km and  $R = 300$  km, we get a total loss of  $\sim 88.7$  dB. Then, the source level (SL) of a 300-km distant source that would be responsible for the measured ANL at 100 Hz would be ( $SL = ANL + TL$ ) 154 dB re  $1 \mu\text{Pa}^2 \text{ Hz}^{-1}$ . Such high noise levels were measured during ice fracturing and ridging events at the observation station. They can certainly occur during the movement of the multi-year ice plume, where the correlation peaked. The large correlation area of  $\sim 500$ -km diameter represents a surface of  $196 \times 350 \text{ km}^2$  from which such high noise events can be recruited to produce the observed ANL in the upper water column sound channel of the Arctic at the mouth of the Amundsen Gulf.

In conclusion, the under-ice ANL in the Eastern Beaufort Sea at the mouth of the Amundsen Gulf appears to be controlled by large-scale ice drift connected to the Beaufort Gyre, and it responds to an average of 7-day wind-forced pulses from the local passing of depressions, which generate a continuous myriad of sources that are summed into a blended background hum at large ranges. The up-slope configuration of the propagation path to the Amundsen Gulf might contribute to the amplification of the signal from 300-km distant sources, recruited over a large  $\sim 200\,000 \text{ km}^2$  area, as schematically represented in Fig. 10.

## ACKNOWLEDGMENTS

Grants are gratefully acknowledged from the Natural Sciences and Engineering Research Council of Canada, the Network of Centres of Excellence ArcticNet, and the Fonds Québécois de Recherche Nature et Technologie to Y.S. and L.F., and from Europôle Mer and exploradoc CMIRA from Région Rhône-Alpes to B.G.K, C.G., and J.I.M.

## APPENDIX: ESTIMATION OF THE AMBIENT-NOISE LEVELS

Estimation of the ambient-noise levels is based on the assumption that the recorded ocean noise is the sum of two independent components following Eq. (A1),

$$m(t) = b(t) + \mu s(t), \quad (\text{A1})$$

where  $b(t)$  is the ambient noise, which is assumed to be Gaussian and stationary for short-term observations ([Urick, 1984](#)),  $s(t)$  is the additional contribution of the distinguishable occasional sources that exceed the ambient-noise level, and the coefficient  $\mu$  is a binary variable that represents the presence ( $\mu = 1$ ) or the absence ( $\mu = 0$ ) of transients signals; The case ( $\mu = 0$ ) has a high probability, close to 1.

The spectral density (power or energy) for a given signal  $s(t)$ ,  $\gamma_s$ , at frequency  $f$  is the Fourier transform (FT) of its autocorrelation function  $\Gamma_s$ , at the time lag  $\tau$ , as given by

$$\gamma_s(f) = \text{FT}\{\Gamma_s(\tau)\}. \quad (\text{A2})$$

As the ambient noise and the transient signal are assumed to be independent, the autocorrelation function of the recorded ocean noise is the sum of the autocorrelation functions of the ambient noise and the transient signals

$$\Gamma_m(\tau) = \Gamma_b(\tau) + \mu^2 \Gamma_s(\tau). \quad (\text{A3})$$

From Eqs. (A2) and (A3), we get

$$\gamma_m(f) = \text{FT}\{\Gamma_b(\tau) + \mu^2 \Gamma_s(\tau)\} = \gamma_b(f) + \mu^2 \gamma_s(f), \quad (\text{A4})$$

where  $\gamma_m(f)$ , the PSD of the acoustic recordings, is a linear combination of two independent PSDs. When faced with real data with finite numbers of measurement points, the PSD is estimated by the periodogram ([Stoica and Moses, 1997](#); [Kay, 1998](#)), following Eq. (A5),

$$\begin{cases} \tilde{\gamma}_m(f) = \frac{1}{Nf_e} |M(f)|^2 = \frac{1}{Nf_e} [\Re e(M(f))^2 + \Im m(M(f))^2], \\ M(f) = \text{FFT}\{m(t)\}, \end{cases} \quad (\text{A5})$$

where  $f_e$  is the sampling rate of the signal,  $N$  is the window length used for the fast Fourier transform (FFT) computation, and  $M(f)$  is the FFT of the measurement  $m(t)$ .  $\Re e$  and  $\Im m$  are the real and imaginary parts of the FFT.

In the absence of transient noise (where  $\mu = 0$ ), the measured PSD [ $\tilde{\gamma}_m(f)$ ] is reduced to the ambient noise periodogram, which can be expressed as the sum of two squared Gaussian random components

$$\begin{cases} \tilde{\gamma}_m(f) = \frac{1}{Nf_e} |M(f)|^2 = \frac{1}{Nf_e} [\Re e(B(f))^2 + \Im m(B(f))^2], \\ B(f) = \text{FFT}\{b(t)\}. \end{cases} \quad (\text{A6})$$

The periodogram [ $\tilde{\gamma}_m(f)$ ] at frequency  $f$  then follows a centralized Chi-2 distribution with two degrees of freedom of mean and variance equal to the true PSD,  $\gamma_m(f)$ .

We attempt to estimate the ambient noise PSD,  $\gamma_m(f)$ , from the spectrogram of a segment of the signal that produces a set of  $\tilde{\gamma}_m(t(i), f)$ ,  $i \in [1, L]$ . For simplicity, let the quantity  $Q$ , a set of discrete values  $Q = \{\tilde{\gamma}_m(t_1, f) \cdots \tilde{\gamma}_m(t_n, f)\}$ , be representative of the ambient-noise distribution, with  $\gamma_m(f)$  as its variance that we aim to estimate. The PDF of this distribution calculated for a given value  $L$  of  $Q$  is

$$f_Q(L) = \frac{1}{\gamma_m(f)} e^{-L/\gamma_m(f)} U(L), \quad (\text{A7})$$

where  $U$  is the step function. The corresponding CDF is

$$F_Q(L) = 1 - e^{-L/\gamma_m(f)} U(L). \quad (\text{A8})$$

The probability  $p$  associated to the  $p$ th percentile ( $q_p$ ) of the assessed  $Q$  values set of the distribution, is then defined by

$$p = 1 - e^{-q_p/\gamma_m(f)}, \quad (\text{A9})$$

which can be transformed into

$$\gamma_m(f) = -\frac{q_p}{\ln(1-p)}. \quad (\text{A10})$$

The above method is applied to the measured acoustic recordings  $m(t)$ , which can contain transient signals merged with ambient noise. As transient signals have high levels relative to ambient noise, by choosing a low percentile value for  $(q_p)$ , we can limit the considered set of  $Q$  values to represent only the ambient noise portion for the estimation of the variance  $\gamma_m(f)$ . This solution was robust for percentile values from 4 to 20%.

In summary, the ambient noise PSD is estimated as follows.

Step 1: choice of the percentile value ( $0.04 \leq p \leq 0.20$ ).

Step 2: choice of the signal segment.

Step 3: spectrogram computation.

Step 4: ascending sorting of each frequency line of the spectrogram.

Step 5: estimation of the value at the chosen percentile.

Step 6: estimation of the PSD of the ambient noise at the frequency bin  $f$ . Repeat for all of the frequency lines of the spectrogram.

<sup>1</sup><http://www.arcticnet.ulaval.ca/> (Last viewed 2013/05/12).

<sup>2</sup><http://www.multi-electronique.com/> (Last viewed 2013/05/12).

<sup>3</sup><http://www.hightechincusa.com/> (Last viewed 2013/05/12).

<sup>4</sup><http://climate.weatheroffice.gc.ca/> (Last viewed 2013/05/12).

<sup>5</sup><http://icdc.zmaw.de/> (Last viewed 2013/05/12).

<sup>6</sup><http://nsidc.org/> (Last viewed 2013/05/12).

Aspin, M. G., Lukovich, J. V., and Barber, D. G. (2009). "Atmospheric forcing of the Beaufort Sea ice gyre: Surface pressure climatology and sea ice motion," *J. Geophys. Res.* **114**, C00A06.

Barber, D. G., Aspin, M. G., Raddatz, R. L., Candlish, L. M., Nickels, S., Meakin, S., Hochheim, K. P., Lukovich, J. V., Galley, R. J., and Prinsenberg, S. J. (2012). "Change and variability in sea ice during the 2007–2008 Canadian International Polar Year program," *Clim. Change* **115**, 115–133.

- Barry, R., Serreze, M., Maslanik, J., and Preller, R. (1993). "The Arctic sea ice-climate system: Observations and modeling," *Rev. Geophys.* **31**, 397–422, doi:10.1029/93RG01998.
- Carey, W. M., and Evans, R. B. (2011). *Ocean Ambient Noise: Measurement and Theory* (Springer, New York), pp. 85–93.
- Fowler, C. (2003). *Polar Pathfinder Daily 25 km EASE-GRID Sea Ice Motion Vectors*, National Snow and Ice Data Center, Digital media, Boulder, CO, USA.
- Galley, R. J., Else, B. G. T., Howell, S. E. L., Lukovich, J. V., and Barber, D. G. (2012). "Landfast sea ice conditions in the Canadian Arctic: 1983–2009," *Arctic* **65**, 133–144.
- Ganton, J., and Milne, A. (1965). "Temperature and wind dependent ambient noise under midwinter pack ice," *J. Acoust. Soc. Am.* **38**, 406–411.
- Greene, C. R., and Buck, B. M. (1964). "Arctic ocean ambient noise," *J. Acoust. Soc. Am.* **36**, 1218–1220.
- Greening, M. V., and Zakarauskas, P. (1992). "A two-component Arctic ambient noise model," *J. Acoust. Soc. Am.* **92**, 2343–2343.
- Greening, M. V., and Zakarauskas, P. (1994). "Spatial and source level distributions of ice cracking in the Arctic Ocean," *J. Acoust. Soc. Am.* **95**, 783–790.
- Kaleschke, L., Heygster, G., Lüpkes, C., Bochert, A., Hartmann, J., Haarpaintner, J., and Vihma, T. (2001). "SSM/I sea ice remote sensing for mesoscale ocean-atmosphere interaction analysis: Ice and icebergs," *Can. J. Rem. Sens.* **27**, 526–537.
- Kay, S. M. (1998). *Detection Theory*, Vol. II of *Fundamentals of Statistical Signal Processing* (Prentice Hall, Upper Saddle River, NJ), pp. 5–13.
- Kimura, N. (2004). "Sea ice motion in response to surface wind and ocean current in the Southern Ocean," *J. Meteor. Soc. Jpn.* **82**, 1223–1231.
- Kwok, R. (2006). "Exchange of sea ice between the Arctic Ocean and the Canadian Arctic Archipelago," *Geophys. Res. Lett.* **33**, L16501.
- Legendre, P., and Legendre, L. (1998). *Numerical Ecology. Developments in Environmental Modeling* (Elsevier, Amsterdam, The Netherlands), Vol. 20, pp. 391–424.
- Lewis, J. K., and Denner, W. W. (1987). "Arctic ambient noise in the Beaufort Sea: Seasonal space and time scales," *J. Acoust. Soc. Am.* **82**, 988–997.
- Lewis, J. K., and Denner, W. W. (1988a). "Arctic ambient noise in the Beaufort Sea: Seasonal relationships to sea ice kinematics," *J. Acoust. Soc. Am.* **83**, 549–565.
- Lewis, J. K., and Denner, W. W. (1988b). "Higher frequency ambient noise in the Arctic Ocean," *J. Acoust. Soc. Am.* **84**, 1444–1455.
- Lukovich, J., Aspin, M., and Barber, D. (2009). "Atmospheric forcing of the Beaufort Sea ice gyre: Surface-stratosphere coupling," *J. Geophys. Res.* **114**, C00A03.
- Makris, N. C., and Dyer, I. (1986). "Environmental correlates of pack ice noise," *J. Acoust. Soc. Am.* **79**, 1434–1440.
- Makris, N. C., and Dyer, I. (1991). "Environmental correlates of Arctic ice edge noise," *J. Acoust. Soc. Am.* **90**, 3288–3298.
- Marsan, D., Stern, H., Lindsay, R., and Weiss, J. (2004). "Scale dependence and localization of the deformation of Arctic sea ice," *Phys. Rev. Lett.* **93**(17), 178501.
- Marsan, D., Weiss, J., Larose, E., and Metaxian, J. P. (2012). "Sea-ice thickness measurement based on the dispersion of ice swell," *J. Acoust. Soc. Am.* **131**, 80–91.
- Maslanik, J., Stroeve, J., Fowler, C., and Emery, W. (2011). "Distribution and trends in Arctic sea ice age through spring 2011," *Geophys. Res. Lett.* **38**, L13502.
- Milne, A., and Ganton, J. (1964). "Ambient noise under Arctic sea ice," *J. Acoust. Soc. Am.* **36**, 855–863.
- Nakayama, Y., Ohshima, K. I., and Fukamachi, Y. (2012). "Enhancement of sea ice drift due to the dynamical interaction between sea ice and a coastal ocean," *J. Phys. Oceanogr.* **42**, 179–192.
- NRC (2003). *Ocean Noise and Marine Mammals* (The National Academy of Sciences, Washington, DC), pp. 1–3.
- Polyak, L., Alley, R. B., Andrews, J. T., Brigham-Grette, J., Cronin, T. M., Darby, D. A., Dyke, A. S., Fitzpatrick, J. J., Funder, S., and Holland, M. (2010). "History of sea ice in the Arctic," *Quaternary Sci. Rev.* **29**, 1757–1778.
- Pritchard, R. S. (1990). "Sea ice noise generating processes," *J. Acoust. Soc. Am.* **88**, 2830–2842.
- Rampal, P., Weiss, J., Dubois, C., and Campin, J.-M. (2011). "IPCC climate models do not capture Arctic sea ice drift acceleration: Consequences in terms of projected sea ice thinning and decline," *J. Geophys. Res.* **116**(C8), C00D07.
- Rampal, P., Weiss, J., and Marsan, D. (2009). "Positive trend in the mean speed and deformation rate of Arctic sea ice, 1979–2007," *J. Geophys. Res.* **114**, C05013.

- Roth, E. H., Hildebrand, J. A., Wiggins, S. M., and Ross, D. (2012). “Underwater ambient noise on the Chukchi Sea continental slope from 2006–2009,” *J. Acoust. Soc. Am.* **131**, 104–110.
- Rotschky, G., Schuler, T. V., Haarpaintner, J., Kohler, J., and Isaksson, E. (2011). “Spatio-temporal variability of snowmelt across Svalbard during the period 2000–08 derived from QuikSCAT/SeaWinds scatterometry,” *Polar Res.* **30**, 5963.
- Smedsrød, L., Sirevaag, A., Kloster, K., Sorteberg, A., and Sandven, S. (2011). “Recent wind driven high sea ice export in the Fram Strait contributes to Arctic sea ice decline,” *Cryosphere Discuss.* **5**, 1311–1334.
- Spreen, G., Kaleschke, L., and Heygster, G. (2008). “Sea ice remote sensing using AMSR-E 89-GHz channels,” *J. Geophys. Res.* **113**, C02S03.
- Stein, P. J. (1988). “Interpretation of a few ice event transients,” *J. Acoust. Soc. Am.* **83**, 617–622.
- Stoica, P., and Moses, R. L. (1997). *Introduction to Spectral Analysis* (Prentice Hall, Upper Saddle River, NJ), pp. 1–14, 23–34.
- Stroeve, J., Serreze, M., Drobot, S., Gearheard, S., Holland, M., Maslanik, J., Meier, W., and Scambos, T. (2008). “Arctic sea ice extent plummets in 2007,” *EOS (Wash. D.C.)* **89**, 13–14.
- Stroeve, J. C., Serreze, M. C., Holland, M. M., Kay, J. E., Malanik, J., and Barrett, A. P. (2012). “The Arctic’s rapidly shrinking sea ice cover: a research synthesis,” *Clim. Change* **110**, 1005–1027.
- Thorndike, A., and Colony, R. (1982). “Sea ice motion in response to geostrophic winds,” *J. Geophys. Res.* **87**, 5845–5852, doi:10.1029/JC087iC08p05845.
- Tsukernik, M., Deser, C., Alexander, M., and Tomas, R. (2010). “Atmospheric forcing of Fram Strait sea ice export: a closer look,” *Clim. Dyn.* **35**, 1349–1360.
- Urick, R. J. (1983). *Principles of Underwater Sound*, 3rd ed. (McGraw-Hill, New York), pp. 169–172.
- Urick, R. J. (1984). “Ambient noise in the sea,” Undersea Warfare Technology Office, Naval Sea System Command, Department of the Navy, Washington, D.C., pp. 3–21, 8-2–8-11.
- Wadhams, P. (2012). “Arctic ice cover, ice thickness and tipping points,” *Ambio* **41**(1), 23–33.
- Weiss, J., Rampal, P., and Marsan, D. (2009). “Acceleration of Arctic sea ice drift and deformation over the last 30 years,” in *IOP Conference Series: Earth and Environmental Science* (IOP, Bristol, UK), Vol. 6, no. 1, p. 012017.
- Xie, Y., and Farmer, D. M. (1991). “Acoustical radiation from thermally stressed sea ice,” *J. Acoust. Soc. Am.* **89**, 2215–2231.
- Xie, Y., and Farmer, D. M. (1992). “The sound of ice break up and floe interaction,” *J. Acoust. Soc. Am.* **91**, 1423–1428.
- Zakarauskas, P., Parfitt, C., and Thorleifson, J. (1990). “Statistiques de bruits ambients transitoires dans l’arctique (Statistics of transient ambient noises in the Arctic),” *J. Phys. Colloq.* **51**, C2-733–C732-736.